New Journal of Physics
The open access journal at the forefront of physics

Deutsche Physikalische Gesellschaft DPG IOP Institute of Physics

Pressure-driven magnetic moment collapse in the ground state of MnO

To cite this article: Deepa Kasinathan *et al* 2007 *New J. Phys.* **9** 235

View the article online for updates and enhancements.

Related content

- Mechanism of magnetic moment collapse under pressure in ferropericlase
  N A Skorikov, A O Shorikov, S L Skornyakov et al.
- Pressure-induced magnetic moment collapse and insulator-to-semimetal transition inBiCoO3
  Xing Ming, Xing Meng, Fang Hu et al.
- Electronic, magnetic and transport properties of rare-earth monopnictides
  Chun-Gang Duan, R F Sabirianov, W N Mei et al.

Recent citations

- Pressure-induced magnetic moment abnormal increase in Mn2FeAl and non-continuing decrease in Fe2MnAl via first principles
  Yang Ze-Jin *et al*
- The local projection in the density functional theory plus U approach: A critical assessment
  Yue-Chao Wang *et al*
- Magnetic transitions in the spin- 52 frustrated magnet BiMn2PO6 and strong lattice softening in BiMn2PO6 and BiZn2PO6 below 200 K
  R. Nath *et al*

This content was downloaded from IP address 194.95.158.35 on 13/06/2018 at 11:07

New Journal of Physics
The open-access journal for physics

Pressure-driven magnetic moment collapse in the ground state of MnO

Deepa Kasinathan[1,3], **K Koepernik**[2,3] **and W E Pickett**[1,4]

[1] Department of Physics, University of California Davis, Davis, CA 95616, USA
[2] IFW Dresden, P O Box 270116, D-01171 Dresden, Germany
[3] Max-Planck-Institut für Chemische Physik fester Stoffe Dresden, Germany
E-mail: wepickett@ucdavis.edu

New Journal of Physics **9** (2007) 235
Received 16 February 2007
Published 17 July 2007
Online at http://www.njp.org/
doi:10.1088/1367-2630/9/7/235

Abstract. The zero temperature Mott transition region in antiferromagnetic, spin $S = \frac{5}{2}$ MnO is probed using the correlated band theory LSDA + U method. The first transition encountered is an insulator–insulator volume collapse within the rocksalt structure that is characterized by an unexpected Hund's rule violating 'spin-flip' moment collapse. This spin-flip to $S = \frac{1}{2}$ takes fullest advantage of the anisotropy of the Coulomb repulsion, allowing gain in the kinetic energy (which increases with decreasing volume) while retaining a sizable amount of the magnetic exchange energy. While transition pressures vary with the interaction strength, the spin-flip state is robust over a range of interaction strengths and for both B1 and B8 structures.

[4] Author to whom any correspondence should be addressed.

PII: S1367-2630(07)44237-9
© IOP Publishing Ltd and Deutsche Physikalische Gesellschaft

The insulator-metal transition (IMT) in correlated systems (the Mott transition) is one of the most actively studied topics in condensed matter systems [1]. The original, and most studied, model is that of the single-band Hubbard model (1HM), characterized simply by bandwidth W and on-site repulsion strength U. Roughly speaking, for $U/W > 1$ it is an insulator characterized by localized states and local moments, while for $U/W < 1$ the system is a non-magnetic metal characterized by itinerant states. In a more general model, the onset of itineracy would lead to increased bonding, hence a volume collapse at the transition. It has recently been emphasized that degenerate multiorbital atoms (N orbitals) with multielectron magnetic moments behave very differently. The critical interaction/bandwidth becomes $(U/W)_c \approx \sqrt{N}$ or even larger [2], due to the increase in conduction (hopping) channels. Another issue is that of a possible orbital selective Mott transition, where only some of the orbitals undergo an IMT transition [3]–[5] depending on the interactions and the anisotropy of the hopping processes.

A much less studied question, one we address here, is how a multielectron local moment disintegrates under reduction of volume. While the moment may be considered to be enforced by the strong interaction U (as in the 1 HM), the inter-orbital Hund's coupling is also a strong factor because it will tend to promote a moment even in the itinerant phase. Anisotropic bonding (hopping processes) causes variation in bandwidths, and the moment collapse may be orbital selective: some but not all orbitals may become spin-paired (doubly occupied), or selected spins may simply flip as the kinetic energy overcomes the Hund's coupling but not the Coulomb repulsion. Pressure-driven collapses of magnetic signals reported in $M^{2+}I_2$ compounds (M = V, Mn, Fe, Co, Ni) [6] and FeO [7], initially interpreted as Mott transitions, have been reinterpreted as magnetic (dis)ordering transitions rather than magnetic collapse [8]. In this paper, we provide predictions for the moment collapse transition in antiferromagnetic (AFM) MnO at $T = 0$, which proceeds by a different route than any yet envisioned.

The Mott transition in MnO at room temperature has recently been revealed through transport [9] and spectroscopic [10, 11] data at high pressure. Occurring entirely within the (spin) disordered phase, there is an insulator–insulator structural transformation B1 (rocksalt) $\rightarrow$ B8 (NiAs) at 90 GPa, followed by an IMT + moment collapse transition at 105 GPa. In fact, this (room temperature) Mott transition at 105 GPa is the first observed for a 3d monoxide. FeO is reported to remain a magnetic insulator to 143 GPa [8]. Unlike for these room temperature experiments where the moments are disordered, the magnetic ground state phases we address will be ordered, and the resulting symmetry lowering [12] and reduced fluctuations are found to affect the character, and probably the mechanism, of the transition.

Previous theoretical work on MnO at reduced volume has been carried out almost entirely in the local spin density approximation (LSDA) and generalized gradient approximation (GGA) [12]–[15]. In these approximations, the small gap at ambient volume rapidly closes leading to metallization at much too small a volume. The resulting occupation of minority t_{2g} states at the expense of majority e_g states leads to a continuous decrease of the calculated moment well before the volume collapse, or moment collapse, transition. Restricted to the B1 structure, GGA gives a metal-to-metal moment collapse from 3.5 to 1.2 μ_B at 150 GPa [13]. The main high pressure phase is expected to be the B8 (NiAs) structure [14], and both the crystal and site symmetry and structural relaxation have been shown to affect predictions strongly [12, 15]. Fang *et al* did apply the LSDA + U method to the high volume phase to improve their picture of the Mott transition.

To study the pressure behaviour of MnO, we have carried out total energy LSDA + U calculations (described below) for both low and high pressure phases. It has recently been

shown that metal-to-insulator transitions, and even charge disproportion and ordering can be modelled realistically with the LSDA + U method [16]. The low pressure structure of MnO is well established: it is an AFM NaCl structure with aligned spins in ⟨111⟩ Mn layers, antiparallel with adjacent layers (AFMII). In our calculations, we have neglected the small rhombohedral distortion angle. There are two simple arrangements of the Mn spins in the B8 phase, ferromagnetic (FM) or AFM. Calculations, including structural optimization, show the AFM phase to be energetically favourable by 0.2 eV per formula unit, for a wide range of pressures.

Results we present below use the LSDA + U method [17] in the rotationally invariant form [18] as implemented in version 5.20 of the full-potential local orbital band structure method (FPLO [19, 20])[5]. The implementation of the LSDA + U method in this code has been provided in detail by Eschrig *et al* [24]. The all-electron aspect of this code is important, since even small-core pseudopotentials cannot reproduce all-electron results under volume reduction [25]. The full-potential aspect can be important also, on the oxygen site as well as on the Mn site, and the non-spherical aspect of the potential will grow as the volume is reduced. Due to the unexpected nature of the reduced spin state, several results were checked, and reproduced, using the Wien2k code [26]. LSDA+U gives two distinct spin states for both B1 and B8 structures: a low pressure high-spin (HS) $S = \frac{5}{2}$ configuration and a high pressure, low-spin (LS) $S = \frac{1}{2}$ state. The equation of state (EOS) curves are displayed in figure 1. From the enthalpies we obtain a first-order magnetic transition from HS-B1 to LS-B1 at $P_{c1} = 123$ GPa, followed by a structural transition to LS-B8 at $P_{c2} = 130$ GPa. The isostructural volume collapse at P_{c1} is $\approx 5\%$. However, these results vary with the choice of U and J (we use 5.5 and 1.0 eV respectively), which is discussed later. This part of our results has been compared with those of other correlated band theory results recently [27]. An unusual feature of the present results is the persistence of the LSDA + U bandgap up to higher pressures, beyond the observed IMT at room temperature [9]. Thus the magnetic and structural transitions we discuss are always insulator-to-insulator, and for the magnetically ordered state at $T = 0$.

To help in understanding the mechanism of the transition, the densities of states (DOS) projected on to each of the $\ell = 2$ irreducible representations are displayed in figure 2, referenced to the rhombohedral axis of the B1 AFMII phase, and equivalently the hexagonal axis of the B8 structure. Not evident from this figure are two potentially important features [28]. Firstly, the 'charge transfer' energy increases as the volume decreases; i.e., the O 2p levels drop in energy relative to the Mn 3d states, reflecting an *increased* tendency toward the fully ionic limit that competes with the increased hybridization as the Mn and O ions approach each other. Secondly, the crystal field splitting between E_g and T_{2g} states increases under pressure, which competes with Hund's exchange and with correlation effects.

In each case the Mn site symmetry splits the 5 d-orbitals into two doublets $e_g^{|m|}$, $|m| = 1, 2$, with $e_g^1 \rightarrow \{xz, yz\}$; $e_g^2 \rightarrow \{x^2 - y^2, xy\}$, and a singlet $a_g \rightarrow 3z^2 - r^2 (m = 0)$. The actual state

[5] A single numerical basis set for the core states (Mn1s2s2p and O 1s) and a double numerical basis set for the valence sector including two 4s and 3d radial functions, and one 4p radial function, for Mn, and two 2s and 2p radial functions, and one 3d radial function, for O was used. The semi core states (Mn 3s3p) are treated as valence states with a single numerical radial function per *nl*-shell. We have used the strong local moment form of the LSDA double-counting correction [17], [21]–[23] that has been become known as the 'atomic-limit' (AL) form (see equation (9) in [23]). The Slater parameters were chosen according to $U = F_0 = 5.5$ eV, $J = \frac{1}{14}(F_2 + F_4) = 1$ eV and $F_2/F_4 = 8/5$.

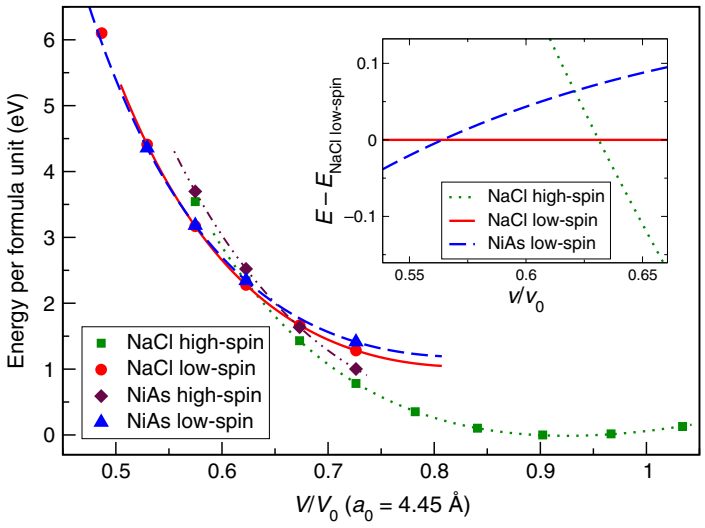

Figure 1. The calculated total energy/MnO versus volume for the low pressure (NaCl) and high pressure (NiAs) structures of MnO. The filled symbols denote the calculated energies and the continuous lines are the least square fitted curves to the Murnaghan EOS for HS and LS configurations respectively. The inset clearly elucidates the order of the transitions, NaCl (HS) → NaCl (LS) → NiAs(LS).

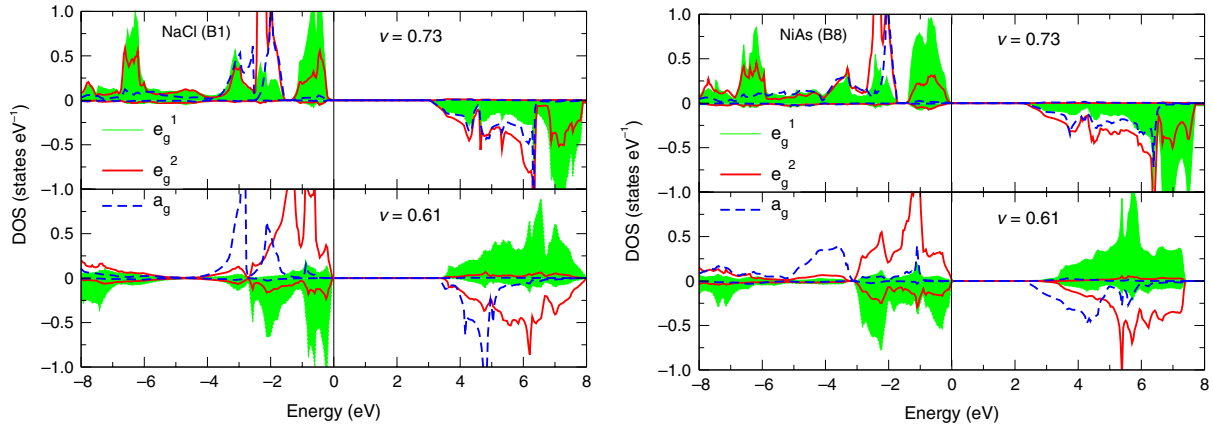

Figure 2. LSDA+U DOS, at the indicated volumes, projected onto symmetrized Mn 3d orbitals in (left panels) the rhombohedral B1 AFMII phase and (right panels) the B8 AFM structure. In each case, the top subpanel is for the HS state, while the bottom is for the LS state. See the text for the definition of the a_g, e_g^1, e_g^2 labels. The overriding feature is the spin-reversal of the $m = \pm 1$ e_g^1 orbitals between the two volumes. Broadening of the a_g states in the LS-B8 DOS is due to the direct Mn–Mn d-overlap in the z-direction in B8 structure (Mn lies on a simple hexagonal sublattice).

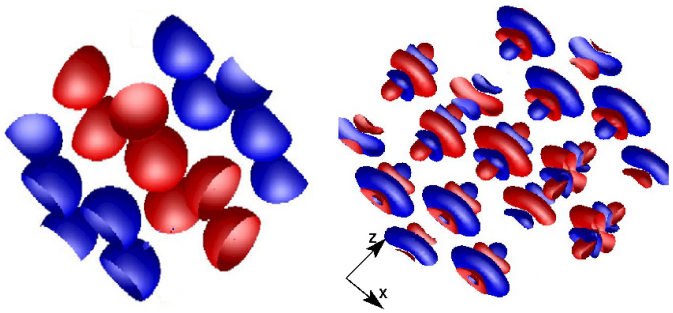

Figure 3. Isosurface plots of Mn ion spin density, with red and blue shading indicating opposite sign. Left: before collapse, showing the spherical $S = \frac{5}{2}$ ion, with (111) layers of aligned spins. Right: after collapse, revealing the anisotropic $S = \frac{1}{2}$ ion. The magnetic order remains AFMII.

realized at a given volume or structure is characterized by two e_g pairs, obtained by unitary mixing, schematically:

$$e_g^a = \cos\beta e_g^1 - \sin\beta' e_g^2, \quad e_g^b = \sin\beta e_g^1 + \cos\beta e_g^2. \tag{1}$$

We have observed and quantified the mixing angle β versus pressure, but near the critical pressure it simplifies to $\beta \approx 0$.

The HS states in both B1 and B8 structures are simple—each 3d orbital is filled once with spins aligned leading to an $S = \frac{5}{2}$ spherical ion. The LS DOS for both structures reveal the essence of the HS–LS transition: the LS state is obtained by simply flipping the spins of the e_g^1 orbitals. This result shows how the LSDA + U method differs in an essential way from LSDA, where the moment decreases continually with volume [13], metallization occurs at low pressure, and decrease of the moment implies rapid collapse of the exchange splitting, resulting in doubly occupied orbitals with zero net spin. In this LS state, each of the 3d orbitals remains singly occupied, the charge density remains spherical while the spin density becomes highly anisotropic, as illustrated vividly in figure 3.

To understand the origin of this spin-flip state, we have performed an analysis of the LSDA + U method. The flavour we have used is the AL [21]–[23]. We consider first the pressure-induced change in kinetic energy relative to the potential energy of the HS and LS states. We first note that the e_g^1 states, whose spins flip in the LS state, are $\frac{2}{3}E_g$ and only $\frac{1}{3}T_{2g}$ in terms of the cubic states we are more familiar with. For the e_g^2 pair this ratio is opposite, and close to the overall mean $(\frac{2}{5}E_g, \frac{3}{5}T_{2g})$. It is the cubic E_g states (and consequently the e_g^1 pair) that have the strongest (dpσ) overlap with O ions, and thus are most affected by pressure and give the greatest gain in kinetic energy.

Now we consider the effects of the very large anisotropy of the LS Mn ion. To separate the effects of U from those of J, we split the energy expression into the isotropic interaction, and the remaining anisotropic part: $E^{\mathrm{AL}} = E^{\mathrm{aniso}} + E^{\mathrm{iso}}$. The isotropic part reads

$$E^{\mathrm{iso}} = \frac{1}{2}(U - J)\sum_s \mathrm{Tr}\left[n^s\left(1 - n^s\right)\right] \geqslant 0, \tag{2}$$

where n^s is the spin-dependent occupation number matrix of the 3d shell, and Tr denotes a trace of the orbital indices. It is easily seen that E^{iso} takes its minima for integer occupations, in

which case we get $E^{\text{iso}} = 0$. However, the resulting potential matrix, to be added to the Kohn–Sham Hamiltonian, is nonzero and has the effect of lowering occupied orbitals by $-\frac{1}{2}(U - J)$, while raising unoccupied orbitals by $\frac{1}{2}(U - J)$. This separation stabilizes insulating magnetic solutions, and also favours HS exchange energy contributions from the magnetic part of the LSDA functional. This tendency opposes the observed HS–LS transition, but operates equally independent of volume. The action of the isotropic term is often the dominating effect of the LSDA + U method, but the common practice of discussing the effects of the LSDA + U method in the isotropic limit misses the physics of this transition, as we now illustrate.

The anisotropic term reads (in the representation in which n^s is diagonal, for simplicity)

$$E^{\text{aniso}} = \frac{1}{2}\sum_{ss'}\sum_{\mu m} n^s_m[\Delta U_{m\mu} - \delta_{ss'}\Delta J_{m\mu}]n^{s'}_{\mu}. \tag{3}$$

The interaction matrix elements are defined as $\Delta U_{m\mu} = w^{m\mu}_{m\mu} - U$, $\Delta J_{m\mu} = w^{\mu m}_{m\mu} - J - (U - J)\delta_{m\mu}$ in terms of the full matrix interaction $w^{m\mu}_{m\mu}$, and these differences do *not* contain U (whose effect is included entirely in the isotropic term). These differences describe *pure anisotropy*; summation of either index of either one gives a vanishing result. Thus a filled spin subshell will not contribute to E^{aniso}, as expected intuitively.

The HS state is favoured by the LSDA spin polarization. However, the LS state still has all fully polarized orbitals, so the energy difference will be much smaller than for usual LSDA $S = \frac{5}{2}$ and $S = \frac{1}{2}$ moments. The resulting ratio of exchange energies can be estimated from the integral over the square of the spin density, which gives a value $E_{1/2}/E_{5/2} \approx 0.31$. This reduction of exchange energy in the LS state is much less dramatic than the estimate from the simple formula $E_x = -\frac{J_{\text{Stoner}}}{4}M^2$. A more detailed explanation of this energy ratio is given in the appendix.

The LS configuration requires the a_g orbital to be singly occupied. The remaining four electrons are then distributed in pairs among the $e_g^{a,b}$ doublets. Analysis shows that the two occupation patterns for which the electrons doubly occupy either the e_g^1 or e_g^2 orbitals have the same anisotropy energy of about $E^{\text{aniso}} \geqslant -0.3J$; a spread of energies arises from allowed mixing of e_g symmetries. The resulting spin density of such states has a_g-derived shape.

The remaining two patterns are obtained by occupying e_g^a in the up-channel and e_g^b in the down-channel or vice versa, both of which results in strongly anisotropic spin densities. The lowest energy of $E^{\text{aniso}} \approx -1.85\,J$ is obtained when the e_g^2 and a_g are occupied in the same spin channel, while e_g^1 is occupied in the opposite channel (note, the mixing angle $\beta = 0$). The other solution ($e_g^{1\uparrow} \parallel a_g^{\uparrow}$) has $E^{\text{aniso}} \approx -1.14\,J$. The dependence of the energies on the mixing angle complicates the discussion.

However, there is a gap of $\approx 0.84\,J$ between the spin-flipped and non-spin-flipped solutions, which is not closed by any mixing. It turns out that this gap is due to the density–density anisotropy (ΔU in equation (3)), which pushes the (density-) non-spherical non spin-flipped patterns up in energy, while it is zero for the (density-) spherical spin-flipped patterns. The exchange and self-interaction-correction contribution to the anisotropy (ΔJ in equation (3)) is nearly of the same size for the non spin-flipped and spin-flipped occupation patterns, and hence does not change the energy separation of these pattern classes. However, it further discriminates the two spin-flipped patterns.

The anisotropy (which is solely controlled by, and proportional to, J in the LSDA+U method) of the interaction favours an occupation pattern which maximizes the spatial distance

between the electrons (under the constraint of $S = \frac{1}{2}$), while the isotropic term $\propto U - J$ merely selects insulating over metallic solutions. We indeed find that both the spin-flipped and non-spin flipped solutions may be found in LSDA + U calculations, separated by an energy of the order derived here. When J is decreased to zero, the energy difference between these solutions shrinks, leaving only the LSDA anisotropy energy difference, which turns out to be very small: about 0.3 eV at ambient pressure and decreasing to zero close to the transition. Of course the LSDA part of the functional includes some anisotropy effects, however the main difference in the influence of the LSDA-anisotropy and the J-anisotropy equation (1) is its action on the Kohn–Sham states. The LSDA potential contributions act on all states, while the LSDA + U potential matrix acts orbital selective. It is this very selectivity, which makes the whole LSDA + U machinery work, by mimicking the suppression of occupation number fluctuations due to correlations. In the same way as the Hubbard band split is not attainable in LSDA, the anisotropy effects are largely suppressed. This suppression is nicely confirmed by the observation of the vanishing energy difference between the two LS solutions as described above.

With increasing pressure the kinetic energy gain becomes more and more competitive with the exchange energy due more to the increasing crystal field splitting than to the bandwidth. This competition usually leads to a (partial) collapse of the magnetic moment. LSDA calculations give a moment of about 1.5 μ_B at our transition pressure, which is far from the HS value of 5 μ_B thus clearly showing that at the transition pressure Hund's first rule is strongly suppressed. In the LSDA + U method, the isotropic term forces the HS solution to have full spin-moment, while the LS solution allows a larger gain in kinetic energy, hence bringing along a transition from HS to LS at some pressure. The anisotropy contribution of LSDA + U is zero for the HS state and negative for the flipped LS state. This will further lower the energy of the flipped LS state against the HS state, resulting in a lower transition pressure. Moreover, this anisotropy contribution is smaller for a non-spin-flipped solution, which rules out this solution. Since the anisotropy term offers a way to keep a sizable amount of magnetic exchange energy, while gaining kinetic energy, it is this 'unusual' state, which is realized after the transition.

We have described here how LSDA + U energies for MnO under pressure predict an unexpected mode of collapse of the Mn moment at zero temperature: each of the 3d orbitals remains polarized, and an $S = \frac{5}{2}$ $-S = \frac{1}{2}$ reduction arises from a simple spin-flip of the symmetry-determined e_g^1 doublet that has the strongest overlap with neighbouring O 2p orbitals. This $S = \frac{1}{2}$ moment in the high pressure phase is consistent with the interpretation of x-ray emission data by Rueff *et al* [11]; Yoo *et al* were less specific about the value of the (clearly small) high pressure moment but presumed total collapse. The partial spin-flip collapse obtained here occurs in both the B1 (rocksalt) and B8 (NiAs) structures, calculated by two different codes, and occurs at similar volumes.

The transition we find is first-order and insulator-to-insulator, both of which insinuate the smallness of fluctuation effects and make the LSDA + U approach an appropriate one. Due to the imprecisely known values of U and J there is an associated uncertainty for the calculated EOS, which depends on the values chosen. The functional dependence of these interaction energies (U, J) on the density is not known and we have neglected the volume dependence. The Wien2k code [26] includes a constrained LSDA algorithm that enables calculation of U, resulting in a value of 6.5 eV for both for the equilibrium volume and close to the transition. To identify the range of variation, we performed EOS calculations for various values of U and J. The resulting transition pressures are depicted in figure 4. As should be expected from the

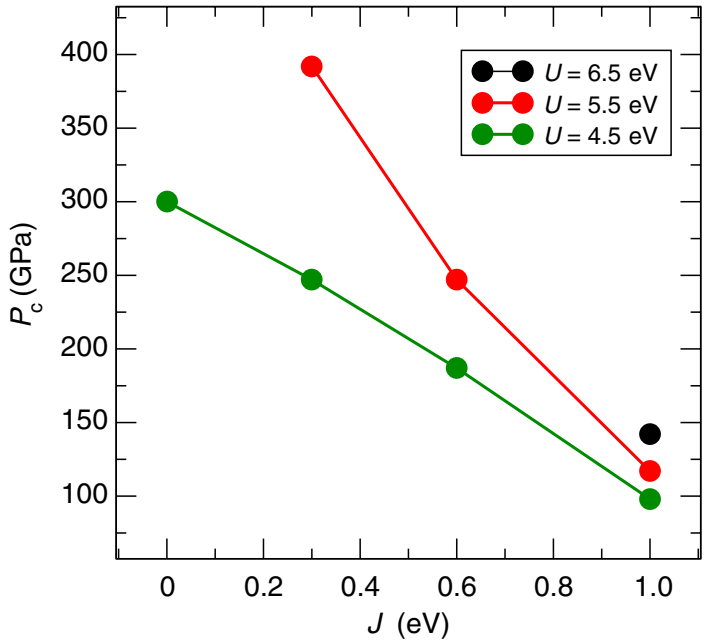

Figure 4. Dependence of the HS to 'spin-flip' LS transition on the parameters, U and J.

importance of the correlation corrections, the transition pressure $P_c(U, J)$ is quite dependent on the parameters. For all values of U, P_c decreases with increasing J. The strong variation confirms our analysis above, which identified the anisotropy (proportional to J) as crucial in determining the ground state at a given volume. The energy separation of the HS and LS curves decreases with J, and this change decreases the transition pressure (the shape dependence of the energy curves on J is minor). On the other hand, the potential matrix element effects (which shift the corresponding eigenvalues) tend to increase the Hubbard splitting with increasing U, which moves to stabilize the HS solution against the LS solution and leads to a monotonic increase of P_c with U. Note that for reasonable values of $J = 0.6$–1 eV, the dependence on U lessens compared to stronger variation for unreasonably small values of J. The very much too large transition pressure for $J = 0$ eV compared to experiment is a strong argument that the anisotropy effects are not sufficiently described by the LSDA part of the functional and hence have to be included in an orbital selective manner.

Although the occupation number fluctuations at this transition should not be a big factor, as the volume is reduced and the bandwidth increases, these fluctuations will tend to increase. The effect can be modelled by adopting a smaller U than the ambient pressure value; hence the value of 5.5 eV that was used for most results presented here becomes justified. On the other hand, the value of J is only weakly screened by the environment, and it is sensible to choose a volume-independent value that resembles the atomic/ionic situation, where one usually finds $J = 0.7$–1 eV for transition metals. Altogether, the calculated transition pressures vary between 100 and 170 GPa for a reasonable choice of J, which is quite satisfactory given the uncertainties of the LSDA + U approach. One should also keep in mind that the zero temperature transition is expected to occur at a higher pressure than at room temperature.

However, we want to stress our main point. Although the LSDA + U method is not capable of precise predictions of P_c due to the uncertainties just discussed, the *spin-flip character* of

the predicted ground state is highly stable against changes of the interaction parameters. For all parameter sets corresponding to the data points in figure 4, we obtain the spin-flip LS solution as the ground state.

Now we summarize: for MnO at $T = 0$ in the AFM ordered phase, an unusual moment collapse $S = \frac{5}{2} \rightarrow \frac{1}{2}$ is predicted before the Mott transition (metallization, or itineracy of the 3d states). These results are robust: the spin-flip state is obtained by two different codes, and for a substantial range of choices of U and J. The value of $U = 5.5\,\mathrm{eV}$ used here corresponds to $U/W \sim 1.5$ in terms of the full 3d bandwidth W. The role of J is central to this transition, but in an unexpected way. Hund's first rule, which is encouraged by the spin-exchange aspect of J, is violated at the transition, whereas the anisotropic Coulomb repulsion that is proportional to J becomes the driving force. Together with an orbitally-dependent increase in kinetic energy, the result is an orbitally-selective spin-flip collapse of the moment at an insulator-to-insulator transition.

The order and type of transitions under pressure we obtain differ from those observed at room temperature [9, 10]. It is established however that structural phase boundaries can be strongly temperature dependent in transition metal oxides [29], so there is no contradiction. The predicted pressure range is accessible to diamond anvil cell experiments, and the ordered-phase moment can be probed by Mössbauer spectroscopy [6].

Acknowledgments

We acknowledge stimulating interaction on this topic with J Kuneš, B Maddox, A K McMahan, R T Scalettar, E R Ylvisaker, and C S Yoo. Work at UCD was supported by Department of Energy grant DE-FG03-01ER45876. This collaboration was stimulated by DOE's Computational Materials Science Network, and we also acknowledge important interactions within the Department of Energy's Stewardship Science Academic Alliances Program. This work was further supported by the Emmy Noether program.

Appendix

The modern flavour of LSDA + U explicitly excludes Hund's first rule from the expression added to the functional, arguing that this contribution is dealt with better within the LSDA part of the functional. In order to obtain estimates of this LSDA-contribution, we will derive an approximate expression for the LSDA xc-energy E_{xc} suitable for the situation we discussed in this paper.

We expand E_{xc} up to second-order in variations of the density. A natural choice for a reference density would be a spherically averaged non-spin-polarized density around the atom centre. We denote the reference density by ρ_0. Our interest is in the effect of different orbital occupations on the magnetic ion. We can describe the spin-density of the l-shell by

$$\rho^s(\mathbf{r}) = \sum_{mn} \phi_{lm}(\mathbf{r}) n^s_{m,n} \phi^*_{ln}(\mathbf{r}),$$

where $n^s_{m,n}$ denotes the generalized occupation number matrix for spin $s = \pm 1$, $\phi_{lm}(r)$ are suitable orbitals and the indices m, n run over the orbitals of the shell. In the usual manner one can write the orbitals as fixed atom-like functions

$$\phi_{lm}(\mathbf{r}) = R_l(r) Y_{lm}(\hat{r}),$$

putting the flexibility into the occupation number matrix. We can introduce the occupation number matrix $\underline{\mathrm{n}} = \sum_s \underline{\mathrm{n}}^s$ for the charge density $\rho(\mathbf{r}) = \sum_s \rho^s(\mathbf{r})$ and the occupation number matrix $\underline{\mathrm{m}} = \sum_s s\underline{\mathrm{n}}^s$ for the magnetization density $m(\mathbf{r}) = \sum_s s\rho^s(\mathbf{r})$. The particle number of the spin channel s is $N^s = \mathrm{Tr}\underline{\mathrm{n}}^s$, which gives the total number of particles as $N = \sum_s N^s$ and the magnetic moment as $M = \sum_s sN^s$. The spherical and spin average of ρ^s is included in the definition of the reference density, hence the density variation due to different occupation patterns is

$$\delta\rho^s(\mathbf{r}) = [R(r)]^2 \sum_{mn} Y_{lm}(\hat{r})\delta n^s_{m,n} Y^*_{ln}(\hat{r}), \tag{A.1}$$

where the variation of the occupation numbers $\delta\underline{\mathrm{n}}^s$ is measured with respect to the averaged occupation numbers ($\Delta = 2l + 1$)

$$n^s_{mn,0} = \delta_{mn}\frac{N}{2\Delta}.$$

Since the reference density is non-polarized the variation of the magnetization density equals the magnetization density itself: $\underline{\mathrm{m}} = \delta\underline{\mathrm{m}}$, $m(\mathbf{r}) = \delta m(\mathbf{r})$.

To keep things simple, we restrict the discussion to the local-density form of the xc-energy

$$E_{\mathrm{xc}} = \int \rho\varepsilon(\rho^+, \rho^-)\,\mathrm{d}^3r.$$

The second-order variational expansion around the reference density then reads

$$E_{\mathrm{xc}} = E_{\mathrm{xc},0} + \int V_{\mathrm{xc},0}(r)\delta\rho(\mathbf{r})\,\mathrm{d}^3r + \int B_{\mathrm{xc},0}(r)m(\mathbf{r})\,\mathrm{d}^3r$$
$$+\tfrac{1}{2}\int \left[P_0(r)(\delta\rho(\mathbf{r}))^2 + 2Q_0(r)(\delta\rho(\mathbf{r})m(\mathbf{r})) + K_0(r)(m(\mathbf{r}))^2\right]\mathrm{d}^3r.$$

The xc-potential and the second-order xc-kernels are spherical due to our spherical reference density ($V_{\mathrm{xc},0}(r) = V_{\mathrm{xc},0}(r)$) and the xc-field is zero, since the reference density is non-polarized. Using this information and the shape of the density variation equation (A.1) we arrive at

$$E_{\mathrm{xc}} = E_{\mathrm{xc},0} + v_0\delta N + \tfrac{1}{2}\sum_{mnm'n'}\left[p_0\delta n_{mn}\delta n_{m'n'} + 2q_0\delta n_{mn}m_{m'n'} + k_0 m_{mn}m_{m'n'}\right]a_{mn,m'n'}$$

with the variation of the particle number $\delta N = \mathrm{Tr}\,\delta\underline{\mathrm{n}}$, with the angular coefficients

$$a_{mn,m'n'} = 4\pi\int Y_{lm}(\hat{r})Y_{ln}(\hat{r})Y_{lm'}(\hat{r})Y_{ln'}(\hat{r})\,\mathrm{d}\Omega, \tag{A.2}$$

and with the radial integrals

$$v_0 = \int V_{\mathrm{xc},0}(r)[R_l(r)]^2 r^2\,\mathrm{d}r, \quad k_0 = \frac{1}{4\pi}\int K_0(r)[R_l(r)]^4 r^2\,\mathrm{d}r, \tag{A.3}$$

$$p_0 = \frac{1}{4\pi}\int P_0(r)[R_l(r)]^4 r^2\,\mathrm{d}r, \tag{A.4}$$

$$q_0 = \frac{1}{4\pi}\int Q_0(r)[R_l(r)]^4 r^2\,\mathrm{d}r. \tag{A.5}$$

For $l \leqslant 2$ and real spherical harmonics we obtain

$$a_{mn,m'n'} = \frac{\Delta}{\Delta+2}\left[\delta_{mn}\delta_{m'n'} + 2\delta_{mn'}\delta_{nm'}\right], \tag{A.6}$$

which leads to the simple expression

$$E_{\mathrm{xc}} = E_{\mathrm{xc},0} + v_0\delta N + \frac{\Delta}{2(\Delta+2)} \times \left[p_0(\delta N)^2 + 2q_0\delta N M + k_0 M^2 2p_0\,\mathrm{Tr}(\delta\underline{\mathrm{n}})^2 + 4q_0\,\mathrm{Tr}(\delta\underline{\mathrm{n}}\underline{\mathrm{m}}) + 2k_0\,\mathrm{Tr}(\underline{\mathrm{m}})^2)\right].$$

In discussing the MnO case, we consider only $3d^5$ occupation patterns, hence $\delta N = 0$. For a spherical magnetic occupation pattern we have to set $\delta n^s_{mn} = \delta_{mn}\frac{sM}{\Delta}$, $\delta n_{mn} = 0$, $\delta m_{mn} = \delta_{mn}\frac{M}{\Delta}$, resulting in $\delta E_{\mathrm{xc}} = \frac{k_0}{2}M^2$, which suggest the interpretation $k_0 = -\frac{I}{2}$ with the Stoner parameter I.

For the HS and spin-flipped LS pattern (SF–LS) we get $\delta\underline{\mathrm{n}} = 0$, since these patterns correspond to a spherical charge density. The magnetic occupation numbers are diagonal and equal to ± 1, hence $\mathrm{Tr}\,\underline{\mathrm{m}}^2 = \Delta$. So we get

$$\delta E^{\mathrm{HS}}_{\mathrm{xc}} = -\frac{I}{4}M^2 = -\frac{I}{4}25,$$

$$\delta E^{\mathrm{SF-LS}}_{\mathrm{xc}} = -\frac{I}{4}M^2 - \frac{I}{4}\frac{2}{\Delta+2}\left(\Delta\,\mathrm{Tr}\,\underline{\mathrm{m}}^2 - M^2\right) = -\frac{I}{4}1 - \frac{I}{4}\frac{48}{7} = -\frac{I}{4}\frac{55}{7}.$$

The SF–LS energy contains a large contribution, which is related to the non-sphericity of the spin-density. It accounts for $\approx 7/8$th of the whole xc-energy of this configuration. The ratio between the energies of these two configurations is $E_{\mathrm{SF-LS}}/E_{\mathrm{HS}} = 11/35 \approx 0.31$.

For the non-spin-flipped pattern (NSF–LS) the diagonal occupation number matrices read $\delta n = (1, -1, 0, -1, 1)$ and $\delta m = (0, 0, 1, 0, 0)$, which gives for the change in xc-energy

$$\delta E^{\mathrm{NSF-LS}}_{\mathrm{xc}} = -\frac{I}{4}M^2 - \frac{I}{4}\frac{2}{\Delta+2}\left(\Delta\,\mathrm{Tr}(\underline{\mathrm{m}})^2 - M^2\right) - \frac{I}{4}\frac{p_0}{k_0}\frac{2\Delta}{\Delta+2}\,\mathrm{Tr}(\delta\underline{\mathrm{n}})^2$$

$$= -\frac{I}{4}1 - \frac{I}{4}\frac{8}{7} - \frac{I}{4}\frac{p_0}{k_0}\frac{40}{7}.$$

Again, the second term is due to the non-sphericity of the spin density. However, it is much smaller than for the flipped case. The third term, proportional to p_0 is related to the non-sphericity of the charge density of the shell. Estimates of p_0 from actual calculations give a value of $p_0 \approx \frac{1}{2}k_0$, hence the third term is roughly of the same size as the sum of the first two terms: $\delta E^{\mathrm{NSF-LS}}_{\mathrm{xc}} \approx -\frac{I}{4}5$, which is only two-thirds of the energy of the spin flipped case.

References

[1] Imada M, Fujimori A and Tokura Y 1998 *Rev. Mod. Phys.* **70** 1039
[2] Gunnarsson O, Koch E and Martin R M 1997 *Phys. Rev.* B **56** 1146
[3] Liebsch A 2004 *Phys. Rev.* B **70** 165103
[4] Fang Z, Nagaosa N and Terakura K 2004 *Phys. Rev.* B **69** 045116

[5] Koga A, Kawakami N, Rice T M and Sigrist M 2004 *Phys. Rev. Lett.* **92** 216402
[6] Pasternak M P and Taylor R D 1993 *Physica* C **209** 113
[7] Pasternak M P and Taylor R D 2001 *Phys. Status Solidi* B **233** 65
[8] Badro J, Struzhkin V, Shu J, Hemley R J, Mao H-K, Kao C-C, Rueff J-P and Shen G 1999 *Phys. Rev. Lett.* **83** 4101
[9] Patterson J R, Aracne C M, Jackson D D, Malba V, Weir S T, Baker P A and Vohra Y K 2004 *Phys. Rev.* B **69** 220101
[10] Yoo C S *et al* 2005 *Phys. Rev. Lett.* **94** 115502
[11] Rueff J-P, Mattila A, Badro J, Vanko G and Shukla A 2005 *J. Phys.: Condens. Matter* **17** S717
[12] Gramsch S A, Cohen R E and Savrasov S Y 2003 *Am. Mineral.* **88** 257
[13] Cohen R E, Mazin I I and Isaak D G 1997 *Science* **275** 654
[14] Fang Z, Terakura T, Sawasa H, Miyazaki T and Solovyev I 1998 *Phys. Rev. Lett.* **81** 1027
[15] Fang Z, Solovyev I V, Sawada H and Terakura K 1999 *Phys. Rev.* B **59** 762
[16] Lee K-W and Pickett W E 2006 *Phys. Rev. Lett.* **96** 096403
[17] Anisimov V I, Zaanen J and Andersen O K 1991 *Phys. Rev.* B **44** 943
[18] Liechtenstein A I, Anisimov V I and Zaanen J 1995 *Phys. Rev.* B **52** R5467
[19] Koepernik K and Eschrig E 1999 *Phys. Rev.* B **59** 1743
[20] Opahle I, Koepernik K and Eschrig H 1999 *Phys. Rev.* B **60** 14035
[21] Anisimov V I, Solovyev I V, Korotin M A, Czyżyk M T and Sawatzky G A 1993 *Phys. Rev.* B **48** 16929
[22] Solovyev I, Dederichs P H and Anisimov V I 1994 *Phys. Rev.* B **50** 16861
[23] Czyżyk M T and Sawatzky G A 1994 *Phys. Rev.* B **49** 14211
[24] Eschrig H, Koepernik K and Chaplygin I 2003 *J. Solid State Chem.* **176** 482
[25] Kolerenč J and Mitas L 2006 *Preprint* cond-mat/0608101
[26] Schwarz K, Blaha P and Madsen G K H 2002 *Comput. Phys. Commun.* **147** 71
[27] Kasinathan D *et al* 2006 *Phys. Rev.* B **74** 195110
[28] Kuneš J private communication
[29] Mao H-K, Shu J, Fei Y, Hu J and Hemley R J 1996 *Phys. Earth Planet. Inter.* **96** 135